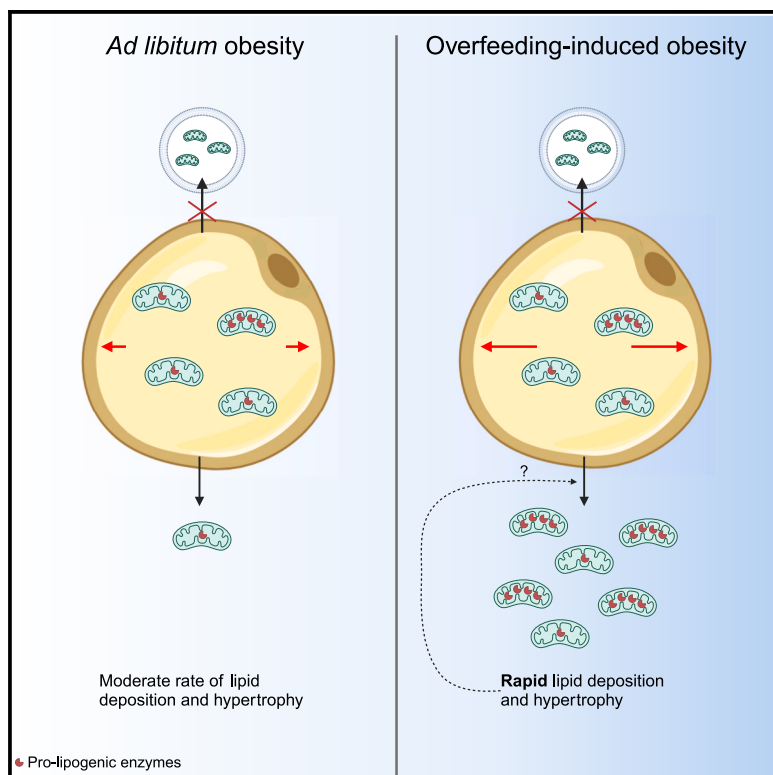


Overfeeding induces adipose tissue release of distinct mitochondria

Graphical abstract



Authors

Joshua H. Goodman, Chloé Berland,
Rajesh K. Soni, Anthony W. Ferrante, Jr.

Correspondence

awf7@columbia.edu

In brief

Goodman et al. demonstrate that adipose tissue from mice with overfeeding-induced obesity has a secreted proteome distinct from equally obese *ad libitum*-fed mice. They additionally find that fat from overfed mice releases intact mitochondria, which are enriched in lipogenic enzymes, suggesting the preferential release of mitochondrial subpopulations.

Highlights

- Overfeeding causes less food intake, rapid fat growth, and less inflammation
- Adipose tissue releases free mitochondria, which is increased by overfeeding
- Overfeeding alters released mitochondria toward a lipogenic mitotype



Article

Overfeeding induces adipose tissue release of distinct mitochondria

Joshua H. Goodman,¹ Chloé Berland,¹ Rajesh K. Soni,^{2,3} and Anthony W. Ferrante, Jr.^{1,4,*}

¹Division of Preventive Medicine & Nutrition, Naomi Berrie Diabetes Center, Columbia University, New York, NY, USA

²Proteomics and Macromolecular Crystallography Shared Resource, Herbert Irving Comprehensive Cancer Center, Columbia University, New York, NY, USA

³Pathology & Cell Biology, Herbert Irving Comprehensive Cancer Center, Vagelos College of Physicians & Surgeons, Columbia University, New York, NY 10032, USA

⁴Lead contact

*Correspondence: awf7@columbia.edu

<https://doi.org/10.1016/j.celrep.2025.115318>

SUMMARY

Overfeeding animals beyond what they eat *ad libitum* causes rapid adipose tissue expansion, leading to an unusual form of obesity characterized by low immune cell accumulation in fat and sustained anorexia. To investigate how overfeeding affects adipose tissue, we studied the protein secretome of fat from equally obese overfed and *ad libitum*-fed mice. Fat from overfed animals secretes lower amounts of immune regulatory proteins. Unexpectedly, fat from overfed mice releases larger amounts of mitochondrial proteins. Microscopy identified mitochondria in the conditioned medium of cultured fat that were found not within extracellular vesicles but rather as free extracellular organelles. The protein profile of released mitochondria was distinct from the mitochondrial protein profile of the whole fat, suggesting that the metabolic stress of overfeeding leads to the release of a mitochondrial subset favoring *de novo* lipogenesis. These findings add to growing evidence that cells alter their energy profiles through the release of mitochondria.

INTRODUCTION

In mammals, the primary function of white adipose tissue is to store excess calories during positive energy balance and efficiently release them when in an energy deficit. Changes in adiposity alter the function and characteristics of adipose tissue, with adiposity modulating the metabolic function of adipocytes, the immune profile of fat, and its secretory and hormonal characteristics.^{1,2} For example, in typical forms of obesity, adipocytes have reduced insulin sensitivity, adipose tissue accumulates large numbers of immune cells, and there is a reduction in the release of some adipokines (e.g., adiponectin) and an increase in others (e.g., leptin).^{3–6} Better characterizing how changes in fat mass alter adipose tissue may provide insights into how its function alters systemic metabolism and behavior.

One unusual form of obesity occurs with overfeeding, i.e., continuing to eat beyond the point of satiety. Normally, body mass is defended so that short-term increases or decreases in fat mass lead to responses that favor a return to the baseline weight.⁷ In both humans and rodents, this leads to an apparent “set point,” from which it is difficult to sustain changes in weight and adiposity.^{8,9} The factors that control and modify the set point are not clear but likely include genetic, developmental, and environmental factors. Enforced weight loss activates a leptin-dependent response that increases hunger, reduces energy expenditures, and improves muscle efficiency.^{9,10} The response to overeating and forced weight gain is much less well understood.

We previously established a mouse model of overfeeding demonstrating a robust response that defends against weight gain and found that leptin is not the signal for this defense response.¹¹

Hypothesizing that adipose tissue is critical for the response that defends against weight gain, we performed histological and transcriptional profiling of adipose tissue from overfeeding-induced obese (OIO) mice and high-fat-diet-fed “*ad libitum* obese” (ALO) animals. An unexpected difference between equally obese OIO and ALO mice was the relative paucity of immune cells, and especially adipose tissue macrophages (ATMs), in adipose tissue from OIO mice. The reason for this is not clear, but previous work has demonstrated that a large fraction of the macrophages that accumulate in obese adipose tissue derive from circulating monocytes that are under the control of adipose-tissue-secreted chemokines, including CCR2 ligands.¹²

More recently, adipose tissue has been found to secrete mitochondria and extracellular vesicles (EVs) in a manner that is modulated by adiposity and lipolysis.¹³ Work is underway to further characterize and understand the role of these secreted products in the physiology of adipose tissue and their contribution to both normal metabolism and the systemic pathology of obesity. Adipocyte-derived EVs have been implicated as key components not only in maintaining local lipid homeostasis¹⁴ but also in the development of obesity-related insulin resistance in the liver and other tissues.¹⁵ Similarly, it has recently been found that intact mitochondria are released from adipocytes



and taken up by local ATMs, as a result of which ATMs modulate their metabolic functioning and lipid catabolism.¹⁶ Additionally, other reports demonstrated that adipocyte-derived mitochondria are taken up by other cell types both locally, including endothelial cells and B cells, and systemically, including cardiomyocytes.¹⁷ One report also claimed that adipocytes release portions of mitochondria in EVs, which make their way into the circulation and affect cardiac injury responses.¹⁸

To better understand how adipose tissue from overfed mice differs from that of weight-stable obese animals, we studied the secretome of fat from overfeeding-induced and ALO mice. There were more than 400 proteins whose release from adipose tissue was altered by overfeeding *per se*. Analysis of these proteins revealed changes in immune-regulatory molecules consistent with histological phenotypes and unexpected alterations in EV-related proteins and mitochondrial proteins. Leptin receptor-deficient (*Lep^{db/db}*) mice were previously predicted to share some characteristics with the overfed mice, and indeed, there was a common effect on the mitochondrial-related secretome. Microscopic analysis identified free mitochondria in the adipose tissue secretome and evidence of free mitochondria in adipose tissue interstitial space and adipocyte endosomes. The proteomic phenotype of the mitochondria (“mitotype”) from overfed adipose tissue appears distinct. While the functional consequence of these findings is not entirely clear, these analyses point to a role for the release of a distinct subset of intact mitochondria as a response to the rapid expansion of adipose tissue.

RESULTS

The secretomes of adipose tissue from *ad libitum* and overfed obese mice are distinct

Although previous studies found that circulating concentrations of several adipose-tissue-derived hormones were not different between overfed and ALO mice, we hypothesized that there would be substantial differences in their secretomes. To characterize how adipose tissue from overfed animals differs from that of ALO mice, we profiled their secreted proteins. Using a previously described overfeeding system,¹¹ we overfed mice with a complete liquid diet through gastric catheters (Figure 1A). The mice were singly housed and given free access to food. Overfeeding led to rapid weight gain, with mice gaining 6.5 ± 2.1 g in 11 days (Figure 1B). To generate equally obese control animals, we provided mice a high-fat diet, which they consumed *ad libitum*. Because ALO mice gain weight at a slower rate than OIO mice, they were begun on the high-fat diet 7 weeks prior to the initiation of overfeeding of OIO mice. During the last 11 days of the experiment (the period of time during which the OIO mice were being overfed), the ALO mice received normal saline via gastric catheters. The overfeeding and saline infusion were stopped after 11 days, all mice were fasted for 24 h, and perigonadal adipose tissue (PGAT) was collected and placed in culture. At the time of sacrifice, the body weights (Figure 1B) and adipose tissue weights (Figure 1C) of the ALO and OIO mice were not different. After 6 h in culture, the conditioned media (CMs) were collected. Standard proteomic analysis using liquid chromatography-tandem mass spectrometry was performed on each sample. 4,522 proteins were detected in total.

As expected, and consistent with their expression being regulated by adipocyte hypertrophy and total fat mass, the concentrations of major adipokines, including adiponectin, leptin, and resistin, were not different between the secretomes of ALO and OIO (Figures 1D and 1F). However, principal-component analysis revealed that the secretomes of OIO and ALO were distinct (Figure 1G). The concentrations of more than 10% of proteins were altered between the secretomes (Figure 1H); the concentrations of 575 were different by more than 50% with a false discovery rate [FDR] < 0.05, including 362 whose concentrations were increased in the OIO adipose tissue secretome compared to that from ALO mice and 213 whose concentrations were decreased. This demonstrates that the products secreted by adipose tissue do not primarily depend on levels of adiposity. As a basis of comparison, an analysis of the difference in CM proteomes between a separate cohort of OIO mice and lean, non-weight-matched mice is included (Figures S1A and S1B).

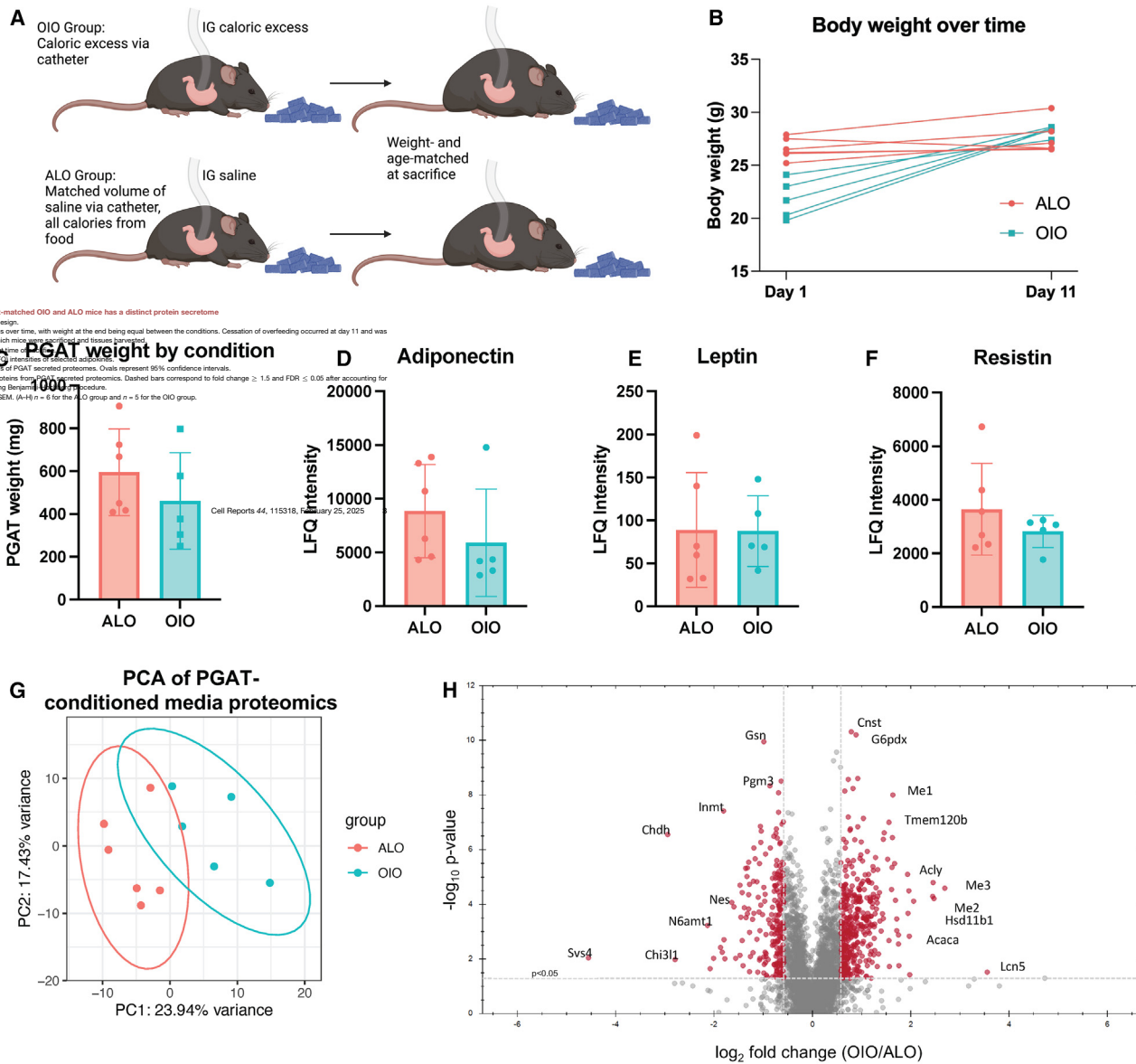
Immune and EV terms are decreased in the OIO protein secretome

To understand programs that were coordinately modulated by overfeeding, we performed unbiased pathway analysis of proteins that were under- or overrepresented in the adipose tissue secretome of OIO compared to ALO mice. Ontology analysis using the Enrichr tool^{19–21} was performed to detect patterns in molecular function, biological process, and cellular localization/compartmentalization. Transcriptional analysis previously found that the expression of inflammatory and chemotactic genes is not induced in OIO adipose tissue, in contrast to ALO adipose tissue, which is characterized by a marked inflammatory expression profile.¹¹ Additionally, infiltration of macrophages into the adipose tissue, normally a hallmark of obesity,⁴ was lower in adipose tissue from OIO mice compared to adipose tissue from ALO mice. Consistent with the previous transcriptional and histological analyses, proteins implicated in chemokine signaling and chemotaxis were reduced in the secretome of adipose tissue from OIO mice compared to that from ALO animals (Figures 2A and 2B). The chemokines that were reduced in the OIO fat secretome compared to ALO included CCL2 and CXCL2, which are required for macrophage¹² and neutrophil²² accumulation in adipose tissue of obese individuals (Figures 2C and 3D).

In typical forms of obesity, the release of EVs by adipose tissue is modulated by fat mass, increasing in more obese individuals.²³ Unexpectedly, functional analysis of the proteins that were lower in concentration in the OIO compared to the ALO secretome suggested that EVs were less abundant in OIO CMs (Figure 2E). Using a nanoparticle tracking analysis platform, we found that, unlike in other forms of obesity, there is a trend toward fewer EVs present in the CMs of PGAT from OIO mice compared to lean controls (Figure 2F). This suggests that adiposity *per se* is not the sole determinant of the rate of EV secretion from adipocytes.

Mitochondrial proteins are enriched in the OIO secretome

To gain insight into which pathways were functionally increased in the secretome of OIO adipose tissue, we performed pathway



analysis of the set of proteins that were more abundant in OIO CMs compared to ALO. Using Gene Ontology terms, 104 distinct biological processes were found to be enriched in the OIO protein secretome, as well as 35 cellular components.^{24,25} Additionally, 185 terms were found to be enriched using the COMPARTMENTS database of protein subcellular localiza-

tion.²⁶ A large number of processes and cellular structures overrepresented in the adipose tissue secretome of the overfed mice pertained to mitochondria and mitochondrial structures and enzymatic pathways (Figures 3A–3C). Of the proteins whose concentrations are higher in OIO compared to ALO adipose CMs, more than half (203/362) are mitochondrial, including 68

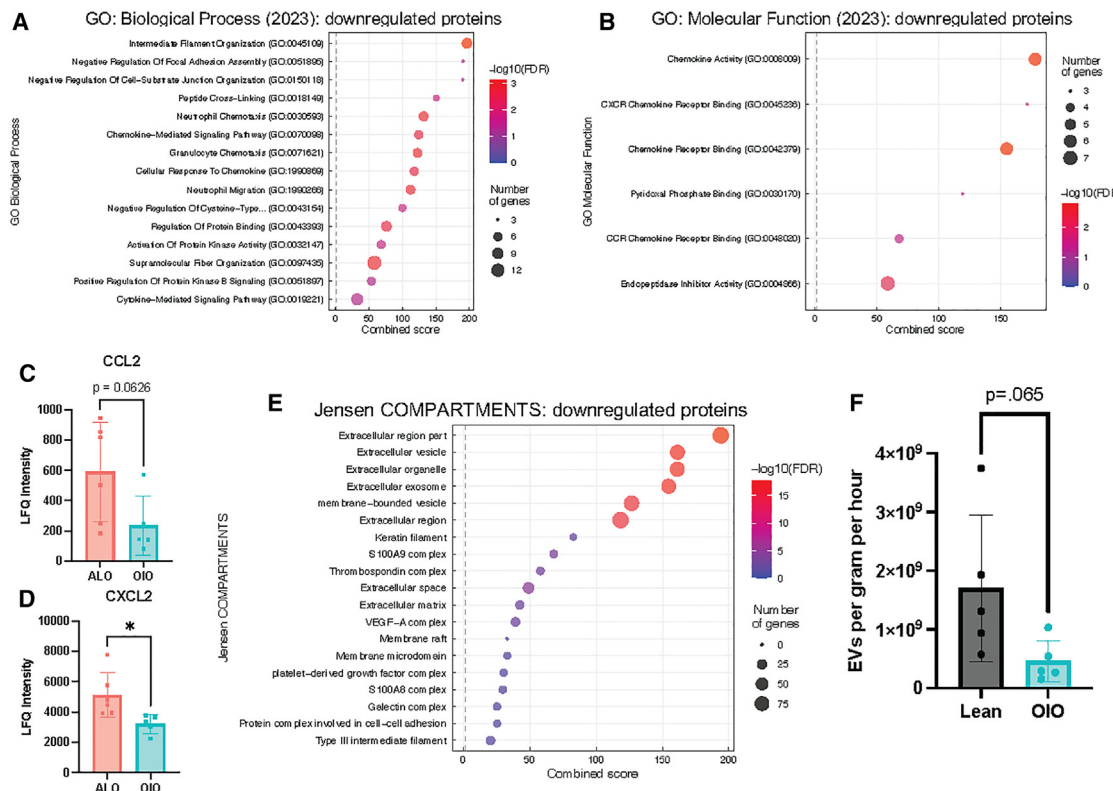


Figure 2. The secretome of OIO PGAT is relatively depleted of chemokines and extracellular vesicles

(A and B) Enrichr analysis of the set of proteins found to be statistically significantly decreased in abundance in OIO conditioned media compared with ALO control.

(C and D) LFQ intensities of selected chemokines.

(E) Enrichr analysis of the set of proteins found to be statistically significantly decreased in abundance in OIO conditioned media compared with ALO control.

(F) Extracellular vesicle abundance as assessed via nanoparticle tracking analysis using the ViewSizer 3000. $n = 5$.

Data are presented as mean \pm SEM. * $p < 0.05$ for Student's t test.

out of the 110 proteins that are increased more than 2-fold. In contrast, only 23 of the 213 proteins downregulated in OIO are mitochondrial, including just 2 out of the 53 proteins decreased more than 2-fold. Ribosomal proteins (13 increased and 2 decreased) and peroxisomal proteins (14 increased and 0 decreased) were also enriched in the OIO secretome. A similar enrichment of mitochondrial and ribosomal proteins was observed in the OIO secretome when compared to lean controls (Figures S1C and S1D). We verified enrichment in mitochondrial protein secretion using a separate cohort of similarly overfed OIO and control ALO mice and showed, via western blot, that the mitochondrial protein HSP60 is increased in the PGAT CMs of OIO vs. ALO mice (Figures 3D and 3E).

Previous reports provided indirect evidence that whole mitochondria are released from adipocytes, and so we measured the abundance of mitochondrial DNA (mtDNA) in the CMs of OIO and ALO adipose tissue. There was a trend toward an increase in mtDNA in the media from OIO compared to ALO tissue (Figure 3F). In contrast, there was no difference in the abundance of extracellular nuclear DNA (Figure 3G). The presence of mtDNA is consistent with mitochondria being released by adipose tissue. Together with the absence of enrichment of proteins

associated with other organelles such as the nucleus, Golgi apparatus, or endoplasmic reticulum (Figure S2), these data suggest that the increase in mitochondrial protein we observed was not merely the result of adipocyte death followed by the indiscriminate release of intracellular contents but rather the result of a process that leads to the specific extracellular release of mitochondrial material. The lack of a consistent increase in the concentration of mtDNA in parallel with increased concentrations of a large number of mitochondrial proteins may reflect an alteration in the mitotype released under these varying conditions.

Mitochondrial components are enriched in the *Lepr*^{db/db} protein secretome

Although the OIO and ALO mice had similar weights, a key distinguishing feature of the OIO model of obesity is the extreme rate of weight gain and adipose tissue hypertrophy. While leptin receptor-deficient (*Lepr*^{db/db}) mice are different from OIO mice in many respects (e.g., body temperature, hunger state, sympathetic tone, and energy expenditure), they are similar in that they gain weight at a far higher rate than mice fed a high-fat diet *ad libitum* and, as previously described, are likely to

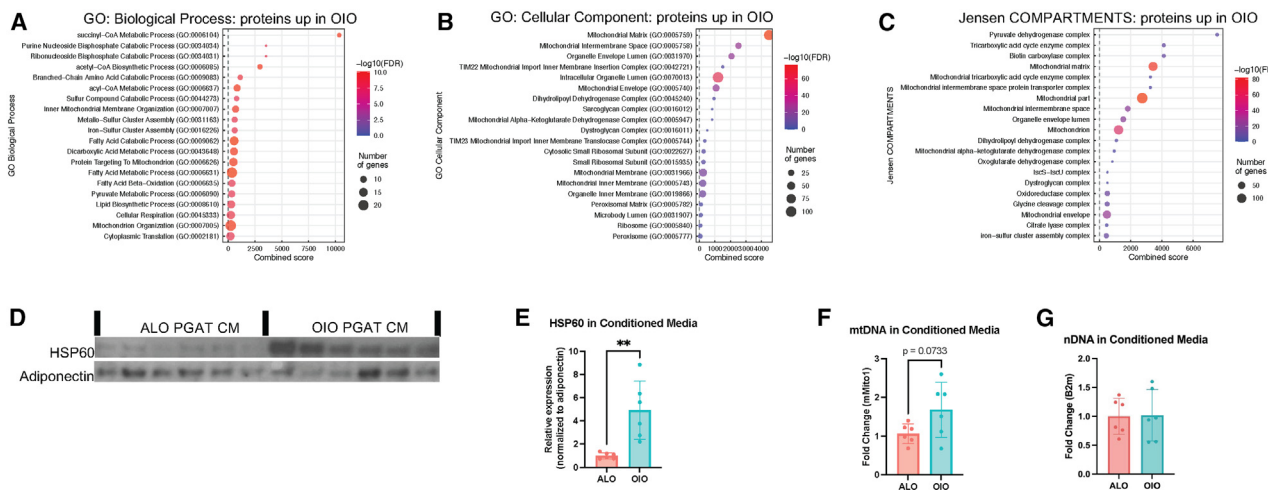


Figure 3. The secretome of OIO PGAT is marked by an increase in mitochondrial material

(A–C) Enrichr analysis of the set of proteins found to be statistically significantly increased in abundance in OIO conditioned media (CMs) compared with ALO control.

(D) Western blot against the mitochondrial protein HSP60 and the non-mitochondrial secreted adipokine adiponectin on PGAT CM from a separate cohort of OIO and ALO mice.

(E) Quantification of the blot in (D).

(F and G) qPCR against the mtDNA gene mMito1 and the nuclear DNA (nDNA) gene B2m on the CM samples. $n = 6$ per condition. Data are presented as mean \pm SEM. ** $p < 0.01$ for Student's t test. (E–G) $n = 6$ per group.

produce an unidentified factor that limits weight gain.⁸ In addition, unlike adipose tissue of OIO obese mice, fat from leptin receptor-deficient mice is highly inflammatory, with large numbers of immune cells, including ATMs. If rapidity of weight gain is responsible for increasing mitochondrial protein release rather than a relative paucity of phagocytic macrophages, then we predicted that we would observe a similar enrichment of mitochondrial proteins in the secretome of adipose tissue from *Lep^{db/db}* mice.

As expected, the secreted proteomes of PGAT of *Lep^{db/db}* mice and weight-matched ALO mice were distinct (Figure 4A). Leptin receptor deficiency more substantially altered the fat secretome than overfeeding, with 1,678 proteins being differentially released by *Lep^{db/db}* adipose tissue compared to that of ALO. 1,187 proteins were increased in abundance and 491 were decreased in the secretome of *Lep^{db/db}* (Figure 4B). Pathway analysis revealed that the pattern of proteins that are released from *Lep^{db/db}* is distinct from that in OIO mice. Nonetheless, a common feature of OIO and the *Lep^{db/db}* adipose tissue secretome is enriched secretion of mitochondrial proteins (Figure 4C). There was not, however, a significant enrichment of mtDNA in the adipose tissue secretome of *db/db* mice (Figures 4D and 4E).

Release of intact mitochondria

Several groups have recently described the release of mitochondria by adipocytes. One group provided visual evidence that only portions of mitochondria are released by adipocytes and contained in exosome-sized vesicles, acting on cardiomyocytes to improve function in response to acute injury.¹⁸ Another group found evidence that adipocytes release functional mitochondria that improve local macrophage function and can be distributed

to distant organs through the circulation.^{16,17} To determine whether any structurally identifiable mitochondria are released by adipose tissue, we analyzed the CM of PGAT by transmission electron microscopy (TEM). Mitochondria were readily identified from various metabolic states, including lean, ALO, *db/db*, and OIO mice (Figures 5A and 5B). The visualized mitochondria encompass a wide range of appearances, though most appear to be somewhat damaged, as would be expected due to processing. Many had lost cristae, some were swollen, and some contained electron-dense deposits or voids. Although cristae morphology was highly variable, outer membranes and inner boundary membranes were visible in nearly all mitochondria. There were no notable differences in mitochondrial size or morphology between conditions. The control mitochondria obtained from healthy cells displayed a similar range of morphologies, consistent with changes induced by processing during isolation (Figure 5A).

We next sought to determine whether we could identify exosomes that contained mitochondrial contents. None were apparent in any electron micrographs. Using size-exclusion chromatography that successfully isolates EVs from adipose-tissue CM, we analyzed the EVs for the presence of mitochondrial proteins and DNA.¹⁴ Using a fluorescent dye that intercalates into lipid bilayers to label all EVs, we did not detect mitochondrial proteins in the fractions that contain EVs (Figures 6A and 6B). mtDNA was present in these fractions, but in the absence of mitochondrial protein, this would be consistent with free mtDNA released as a result of a breakdown of released mitochondria. Consistent with the presence of intact mitochondria too large to enter the gel matrix, the majority (53%) of mtDNA in the CM did not pass through the column.

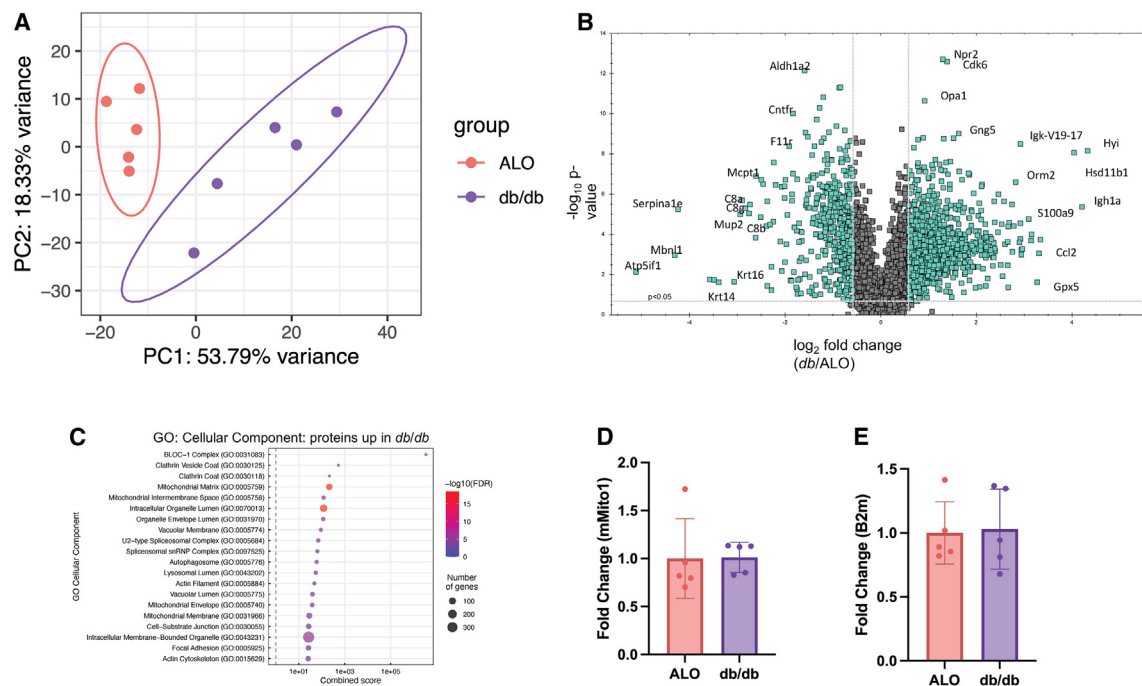


Figure 4. The protein secretome of db/db PGAT is distinct from that of ALO and enriched in mitochondrial peptides

(A) Principal-component analysis of PGAT secreted proteomes. Ovals represent 95% confidence intervals.

(B) Volcano plot of individual proteins from PGAT secreted proteomics. Dashed bars correspond to fold change ≥ 1.5 and FDR ≤ 0.05 after accounting for multiple comparison testing using Benjamini-Hochberg procedure.

(C) Enrichr analysis of the set of proteins found to be statistically significantly increased in abundance in db/db conditioned media compared with ALO control.

(D and E) qPCR against the mtDNA gene mMito1 and the nDNA gene B2m on the conditioned medium samples. $n = 5$ per condition.

Data are presented as mean \pm SEM. $n = 5$ per group.

To assess whether we could detect extracellular mitochondria in intact adipose tissue, we performed TEM on PGAT of obese mice. Intracellular mitochondria were readily identified in both adipocytes and non-adipocytes, with the adipocyte mitochondria appearing more electron dense and oblong (Figure 6C). In addition, mitochondria were seen in the extracellular space between cells (Figure 6C). Unexpectedly, within some adipocytes, we identified mitochondria within endosomes (Figure 6D). These endosomes also appeared to contain particles consistent with previously reported lipid-laden EVs. These micrographs suggest that extracellular mitochondria exist in adipose tissue and provide a possible pathway—endosomal release—for release from adipocytes. However, we have not demonstrated that the mitochondria that we detect are in fact specifically released from adipocytes.

Several groups have reported that adipocyte-derived mitochondria are efficiently taken up by macrophages. To test whether the extracellular mitochondria released by adipose tissue that we detect can be similarly taken up, we labeled mitochondria released from adipose tissue with a fluorescent dye (PKH26) that intercalates into lipid bilayers. As a positive control, we labeled adipocyte-derived EVs with the same dye. As previously reported, adipocyte-derived EVs are efficiently taken up by bone marrow-derived macrophages, labeling nearly all macrophages uniformly (Figure 6E). Similarly, adipose-tissue-derived mitochondria fluorescently labeled with PKH26 were taken up

by macrophages so that nearly all macrophages fluoresced (Figure 6E). However, whereas the fluorescence of macrophages that phagocytosed EVs was maximally labeled, there was variation in the fluorescence of macrophages labeled by the mitochondria, arguing that the number of EVs was significantly greater than that of extracellular mitochondria.

Mitochondria released by overfed animals have a distinct protein profile

Recently, it has been recognized that there are different classes of mitochondria that can be distinguished by their functions, e.g., steroid synthesis, heat production, and reactive oxygen species production.²⁷ The identity of these different types of mitochondria—mitotypes—are reflected in part by their varied protein content. We observed that the large majority of mitochondrial proteins identified were more abundant in the OIO secretome (Figure 7A) but wanted to assess whether particular mitotypes were enriched within this population. Using gene set enrichment analysis,²⁸ we asked whether any mitochondrial pathways or functional classes of proteins were overrepresented among the mitochondrial proteins differentially detected between conditions. While 27 mitochondrial pathways²⁹ were found to be enriched (Table S1), lipid metabolism was found to have the highest normalized enrichment score (Figure 7B).

The relative increase in abundance of individual proteins in the OIO compared to the ALO CM was not equal for all

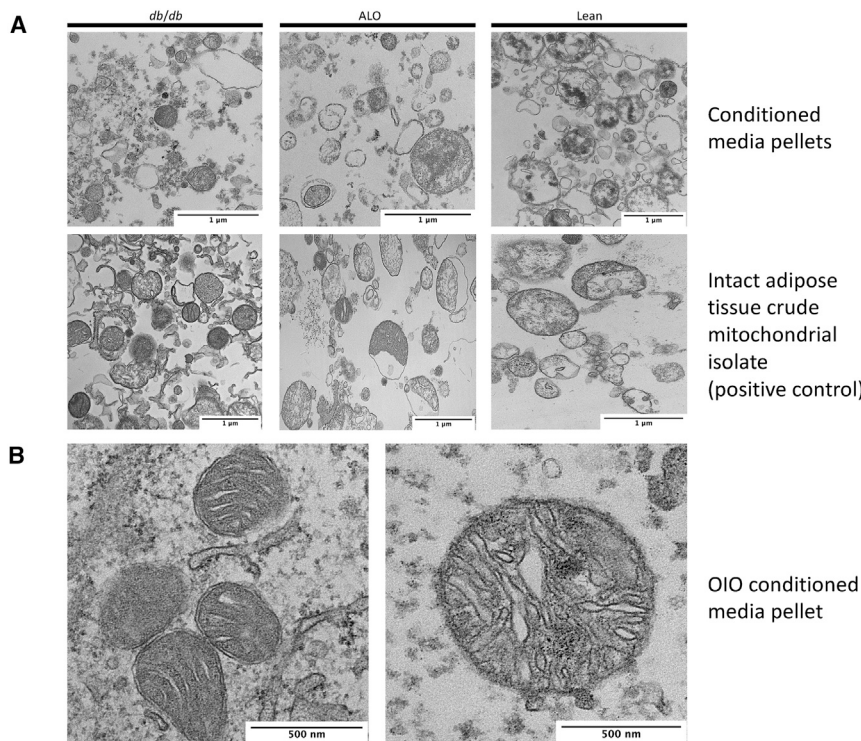


Figure 5. Adipose tissue secretes ultrastructurally intact mitochondria

(A) Images showing a range of morphologies of ultrastructurally intact mitochondria collected from conditioned media (top) and intact cells (bottom) across a range of metabolic states. (B) Detailed images of mitochondria collected from conditioned media of OIO PGAT.

DISCUSSION

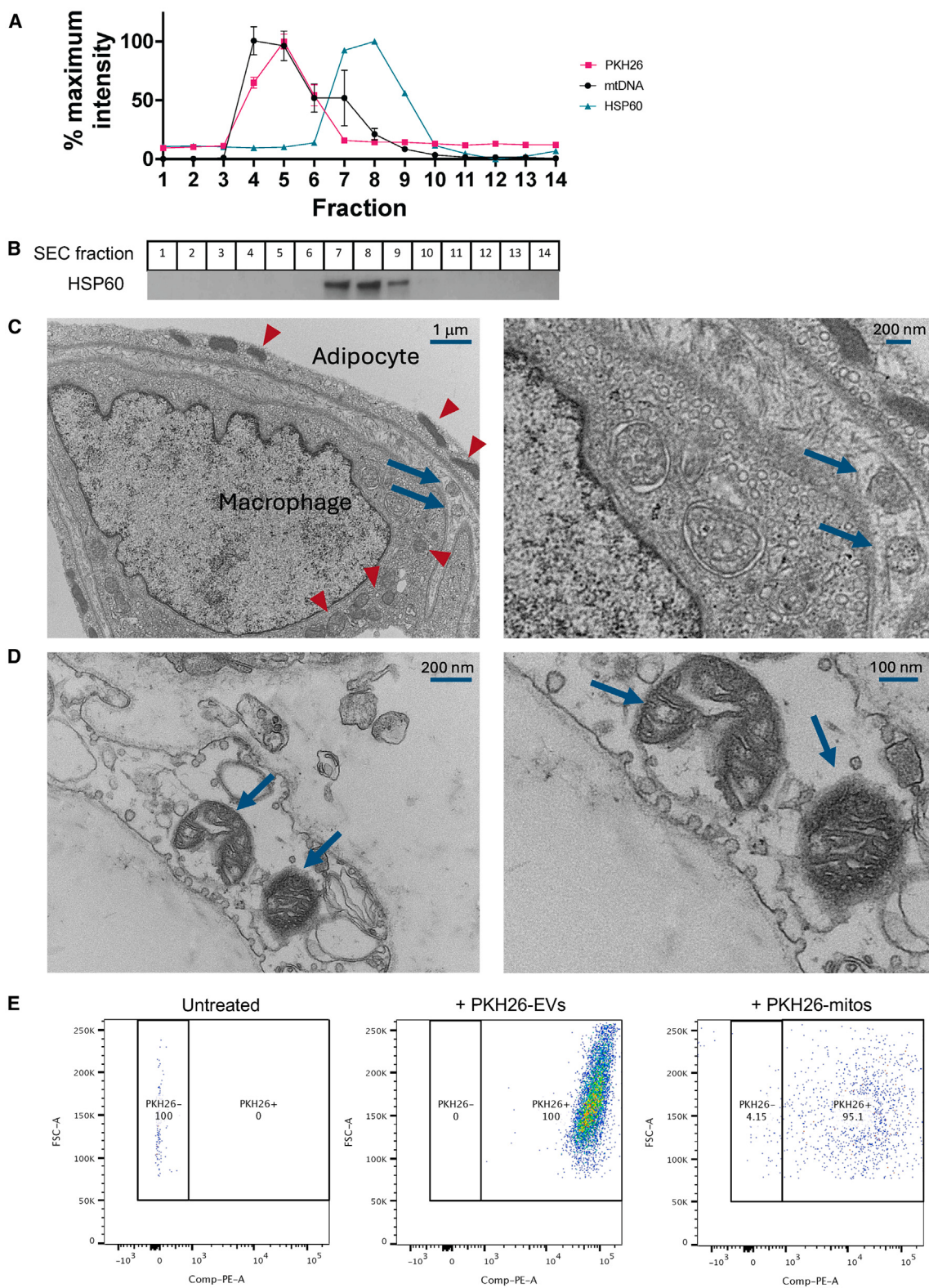
Since the initial discovery of intercellular mitochondrial transfer nearly 20 years ago,³³ a growing body of research has slowly emerged, identifying and characterizing extracellular release of mitochondria.³⁴ Much is unknown, but what has become clear is that the release of mitochondria occurs in several different forms—from secretion in EVs to transport via nanotubes. Several recent studies^{16–18,35} have revealed that adipocytes release mitochondria or portions of mitochondria that then act to alter local and distant cell functions. Studies by Brestoff and colleagues have documented the transfer of adipocyte mitochondria to local ATMs in a process

peptides. Among all differentially expressed mitochondrial proteins, the median was 1.8 times more abundant in the OIO condition, but some proteins were enriched by 4-fold or more. Consistent with the preferential release of a particular mitotype, several of the enzymes necessary for fatty acid production were among the most increased in abundance in OIO CMs. Specifically, the family of malic enzymes (ME1–3), critical for the generation of NADPH and NADH and for fatty acid synthesis,^{30–32} were 3–5 times more abundant in the OIO compared to the ALO secretome (Figure 7C). Similarly, ATP-citrate lyase (encoded by the gene Acly) and acetyl-coenzyme A (CoA) carboxylase 1 alpha (Acaca), which are required for malonyl-CoA synthesis, were increased 3.8- and 3.9-fold, respectively. In contrast, the enzymes that form the citric acid cycle, which provides an alternative fate for acetyl-CoA, were, on average, increased only 1.9-fold. Collectively, these data suggest that while mitochondrial enzymes across a range of metabolic processes are increased in the OIO secretome, secreted mitochondria are particularly poised to perform *de novo* lipogenesis.

We confirmed that malic enzymes 1 and 2 are both highly up-regulated in OIO CMs compared with ALO via western blot (Figures 7D and 7E). This was not due to higher expression of these proteins in OIO adipose tissue (Figures 7F and 7G). Together, these results suggest that the increased release of mitochondrial content in the OIO state, and particularly of mitochondria enriched in pro-lipogenic enzymes, is due to preferential release of particular mitochondrial subtypes rather than enhanced release of all mitochondrial content.

that alters the metabolic function of the recipient cells. Scherer and colleagues have found evidence of portions of mitochondria contained within adipocyte-derived EVs that function to alter cardiomyocyte response to injury. Bernlohr and colleagues, on the other hand, found evidence of mitochondrial proteins in some adipocyte-derived EVs but not intact mitochondria *per se*. In this study, we present the first electron microscopy confirmation of intact mitochondria being released from white adipose tissue and evidence that the release of distinct mitochondrial subtypes is based on the metabolic state of adipose tissue.

Our observation that the mitochondria released from adipose tissue in the setting of intragastric overfeeding are preferentially enriched for enzymes that perform *de novo* lipogenesis suggests that the release of different mitochondrial populations may be adaptive; the overfed state is one of extreme caloric excess and high intracellular triglyceride stores within adipocytes, so there is presumably little need for the generation of new fatty acids. It may, therefore, be favorable to the cell to release this population of mitochondria that is primed to perform an unnecessary task. Such a phenomenon could potentially increase the cells' fitness for a variety of reasons, including biomechanical and energetic ones. For example, the cell membrane is mechanically stressed by the hypertrophy that results from the rapid expansion of lipid droplets, and release of mitochondria could serve to decrease intracellular volume and relieve biomechanical stress. Additionally, it is likely more efficient to dispose of unneeded mitochondria via extracellular release rather than via energetically



(legend on next page)

intensive lysosomal recycling; it is already known that ATMs catabolize adipocyte-derived lipids within their lysosomes,^{36,37} raising the possibility that a similar process could occur with mitochondria. However, while we do observe an increase in mitochondrial proteins and observe mitochondria in the secretome of *Lepr^{db/db}* adipose tissue, the protein profile of the mitochondria is distinct from that of the OIO released mitochondria (i.e., few differences in *de novo* lipogenesis enzymes), suggesting that multiple aspects of the metabolic state govern the phenotype of released mitochondria.

The finding that overfed adipose tissue preferentially releases mitochondria with a particular mitotype raises an additional question unanswered by previous studies regarding intercellular mitochondrial transfer. While some studies have examined the effect of the metabolic state on the rate of release of mitochondrial content,³⁵ little has been done to characterize differences in the functional or proteomic identity of the released mitochondria themselves across different physiological states. Thus, there remain significant questions regarding the applicability of previous findings regarding the functional effect of uptake of secreted mitochondria across physiological states dissimilar to those explicitly studied.

A major outstanding question regards the fate of the *de novo* lipogenesis-poised mitochondria that we identify as preferentially released from overfed adipose tissue, as well as any potential effects these mitochondria exert on recipient cells. We have demonstrated *in vitro* that macrophages do efficiently take up the adipose-tissue-released mitochondria, but the fate of these organelles *in vivo* is not clear. Previous work has found that locally released extracellular mitochondria are taken up by ATMs. While we have not addressed these questions in the current study, it will provide a rich avenue of research in the future.

Taken together, our data help confirm as well as complicate a series of recent studies regarding mitochondrial release from adipose tissue. We show direct evidence of the release of ultrastructurally intact mitochondria from adipose tissue via electron micrographs, though we find no evidence of mitochondria or mitochondrial fragments contained within EVs. We demonstrate that the release of mitochondria from adipose tissue is increased in the setting of intragastric overfeeding when compared to weight-matched controls and, additionally, that the released mitochondria are functionally enriched in enzymes related to fatty acid synthesis. We also confirm our previous observations that adipose tissue from overfed mice represents a non-inflammatory state of obesity. Taken together, these findings suggest that a better understanding of the

overfed obese state and adipose tissue mitochondrial release could help improve our understanding of obesity-associated disease.

Limitations of the study

Disparities between our findings and those of other groups regarding the presence of mitochondrial components within EVs may potentially result from differences in methodologies used to isolate vesicles. While we use a technique that relies on size-exclusion chromatography, methodologies that employ ultracentrifugation or commercially available isolation kits may enrich different subpopulations of vesicles. It is also possible that some differences may result from the fact that other studies have examined vesicles from the culture of adherent adipocytes differentiated from immortalized pre-adipocytes, whereas we utilize intact pieces of primary tissue. As a result of using primary tissue, we are also unable to definitively claim that the mitochondria are derived from adipocytes rather than stromal cell populations present within the adipose tissue compartment.

An important dimension of adipose tissue complexity that our study does not address is depot specificity. We utilized murine PGAT for our studies because it is well characterized and thought to contribute directly to obesity-related metabolic disease.^{38,39} Thus, it is possible that the mitochondrial secretome (as well as the broader protein secretome) of subcutaneous fat is biologically distinct from that of visceral fat, particularly given its potentially anti-inflammatory and neuroprotective roles in obesity.^{40,41} Additionally, conclusions should not be drawn regarding the applicability of these findings to humans, especially given the differences in physiology that have been found between murine and human visceral adipose depots.^{39,42} However, preliminary experiments (data not shown) show that an enrichment in *de novo* lipogenesis enzymes is similarly seen when analyzing the secretome of adipose tissue from overfed female mice, suggesting that at least some of the effects we observe are not sex dependent.

Lastly, the dietary makeup and timing of nutrition is necessarily different between the overfeeding condition and other conditions, which inherently complicates any direct comparison between groups. The diets of the OIO and ALO groups are not perfectly matched in terms of macronutrient makeup, and factors like timing of food ingestion and post-oral sensation are also necessarily different due to the technical limitations of the system. While including *Lepr^{db/db}* and lean mice in our analyses helps to control for some of these factors, it is impossible to completely disentangle these variables.

Figure 6. Most mitochondrial components in conditioned media are not found within extracellular vesicles and are adipocyte derived

- (A) Abundance across size-exclusion chromatography (SEC) fractions of adipose tissue conditioned-medium-derived exosomes as quantified by PKH26 fluorescence (pink), mtDNA as quantified via qPCR against mMito1 (black), and HSP60 as quantified via western blot shown in (B) (blue). All values are normalized relative to the maximal value among SEC fractions.
- (B) Western blot against HSP60 within SEC fractions.
- (C) Transmission electron micrograph of PGAT. Elongated intracellular mitochondria are visible in adipocytes and a macrophage (arrowheads). Oval extracellular mitochondria are seen in the interstitial space between cells (arrows).
- (D) Transmission electron micrograph of endosome in an epididymal adipocyte. Intraluminal mitochondria (arrows) and budding extracellular vesicles are visible.
- (E) Flow cytometric analysis of bone marrow-derived macrophages (BMDMs) supplemented with PKH26-labeled adipose-tissue-derived extracellular vesicles (EVs) and PKH26-labeled adipose-tissue-derived mitochondria.

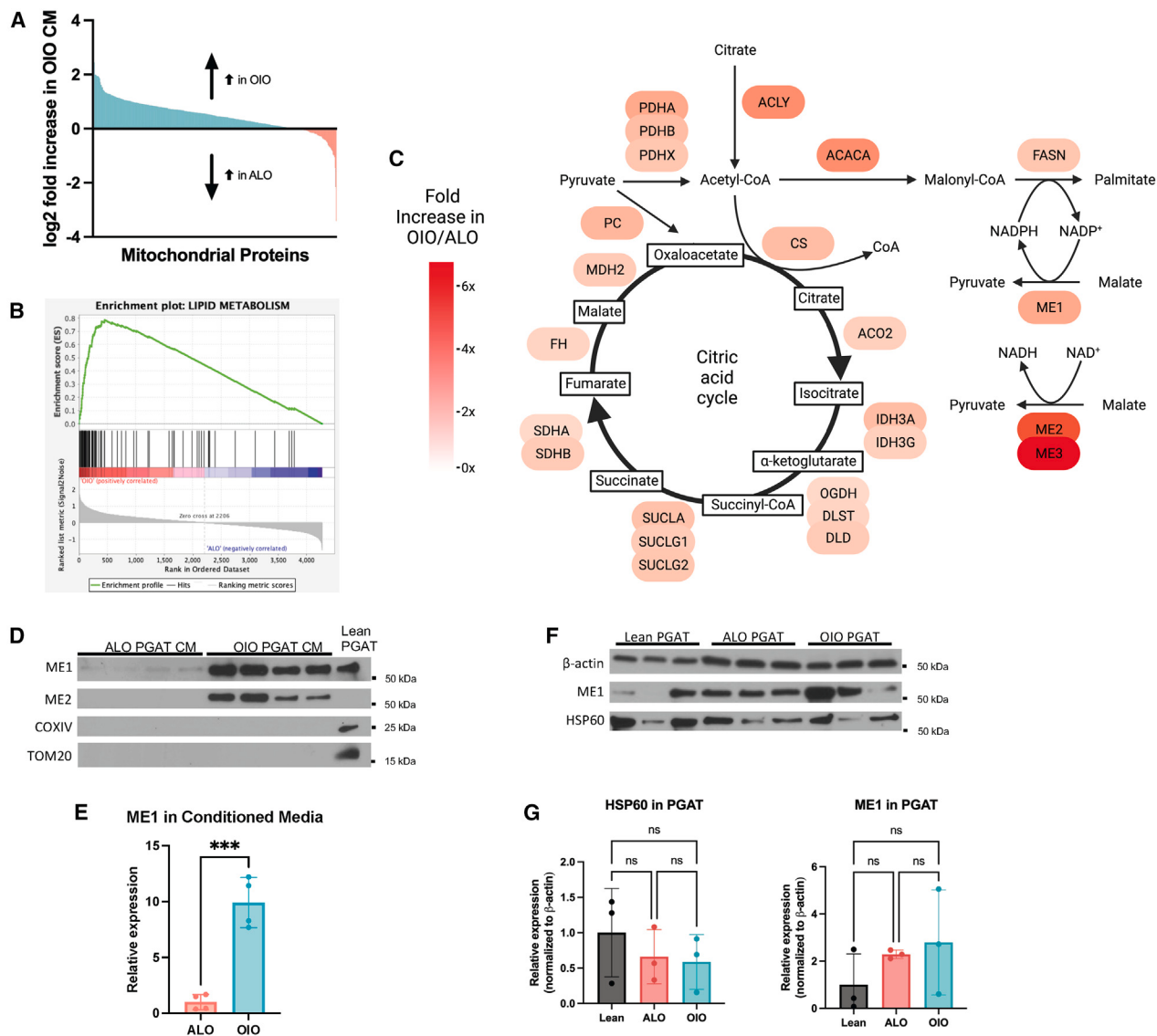


Figure 7. Adipose tissue from overfed mice differentially secretes mitochondria enriched for anabolic functioning
(A) Waterfall plot of the average fold change in expression levels of all MitoCarta3.0-annotated mitochondrial proteins detected in OIO and ALO conditioned media, log₂ transformed.

(B) GSEA enrichment plot for the MitoCarta3.0 term "lipid metabolism" on proteins increased in OIO CM.

(C) Schematic of *de novo* lipogenesis and TCA cycle enzymes and their relative enrichment in OIO vs. ALO CM.

(D and E) Western blots of conditioned media from ALO and OIO PGAT and control whole lean PGAT.

(F) Western blots of whole PGAT from lean, ALO, and OIO mice.

(G) Quantification of western blots in (F).

Data are presented as mean ± SEM. ***p < 0.001 for Student's t test.

RESOURCE AVAILABILITY

Lead contact

Requests for further information and resources should be directed to the lead contact, Anthony W. Ferrante, Jr. (awf7@columbia.edu), who will handle and respond to them accordingly.

Materials availability

This study did not generate new unique reagents.

Data and code availability

Proteomics data have been uploaded to ProteomeXchange via the Proteomics Identification Database EMBL-EBI (PRIDE) and are accessible under the identifiers PRIDE:PXDO51294 (*Lepr*^{db/db} data) and PRIDE:PXDO51296 (OIO data).

ACKNOWLEDGMENTS

This study was supported by research grants to A.W.F. from the NIH (R01DK066525) and Boehringer-Ingelheim Pharmaceuticals Fellowship and

training support was provided to J.H.G. from the NIH (F30DK129008 and T32GM007367) and to C.B. from the Russell Berrie Foundation. We thank Kun-heng Cai for assistance with EV quantification. We thank Martin Picard and members of the Picard lab for advice and suggestions regarding mitochondrial biology. We thank Lee Cohen-Gould and Juan Jimenez of the Weill Cornell Microscopy and Image Analysis Core Facility for their assistance with TEM.

AUTHOR CONTRIBUTIONS

All experiments were conceived of and designed by J.H.G. and A.W.F., and all experiments were carried out by J.H.G. C.B. designed and carried out murine overfeeding experiments. R.K.S. performed and analyzed the proteomics experiments. The manuscript was written by J.H.G. and A.W.F.

DECLARATION OF INTERESTS

This work was partially funded by a research grant from Boehringer-Ingelheim Pharmaceuticals to A.W.F.

STAR METHODS

Detailed methods are provided in the online version of this paper and include the following:

- KEY RESOURCES TABLE
- EXPERIMENTAL MODEL AND STUDY PARTICIPANT DETAILS
 - Animals and animal care
 - Adipose tissue culture
 - Macrophage culture
- METHOD DETAILS
 - Surgery
 - Intragastric tube preparation
 - Overfeeding protocol
 - Processing of conditioned media
 - Global quantitative proteomics analysis
 - LC-MS/MS
 - Exosome enrichment
 - Nanoparticle tracking analysis
 - Western blot
 - qPCR
 - Electron microscopy
 - Flow cytometry
 - Figures
- QUANTIFICATION AND STATISTICAL ANALYSIS

SUPPLEMENTAL INFORMATION

Supplemental information can be found online at <https://doi.org/10.1101/2025.11.15.5318>.

Received: June 19, 2024

Revised: November 20, 2024

Accepted: January 24, 2025

Published: February 18, 2025

REFERENCES

1. Uchi, N., Parker, J.L., Lugus, J.J., and Walsh, K. (2011). Adipokines in inflammation and metabolic disease. *Nat. Rev. Immunol.* 11, 85–97. <https://doi.org/10.1038/nri2921>.
2. Kawai, T., Autieri, M.V., and Scalia, R. (2021). Adipose tissue inflammation and metabolic dysfunction in obesity. *Am. J. Physiol. Cell Physiol.* 320, C375–C391. <https://doi.org/10.1152/ajpcell.00379.2020>.
3. Ferrante, A.W. (2013). The Immune Cells in Adipose Tissue. *Diabetes Obes. Metabol.* 15, 34–38. <https://doi.org/10.1111/dom.12154>.
4. Weisberg, S.P., McCann, D., Desai, M., Rosenbaum, M., Leibel, R.L., and Ferrante, A.W. (2003). Obesity is associated with macrophage accumulation in adipose tissue. *J. Clin. Invest.* 112, 1796–1808. <https://doi.org/10.1172/JCI19246>.
5. Arita, Y., Kihara, S., Ouchi, N., Takahashi, M., Maeda, K., Miyagawa, J., Hotta, K., Shimomura, I., Nakamura, T., Miyaoka, K., et al. (1999). Paradoxical Decrease of an Adipose-Specific Protein, Adiponectin, in Obesity. *Biochem. Biophys. Res. Commun.* 257, 79–83. <https://doi.org/10.1006/bbrc.1999.0255>.
6. Klein, S., Coppack, S.W., Mohamed-Ali, V., and Landt, M. (1996). Adipose Tissue Leptin Production and Plasma Leptin Kinetics in Humans. *Diabetes* 45, 984–987. <https://doi.org/10.2337/diab.45.7.984>.
7. Leibel, R.L., Rosenbaum, M., and Hirsch, J. (1995). Changes in Energy Expenditure Resulting from Altered Body Weight. *N. Engl. J. Med.* 332, 621–628. <https://doi.org/10.1056/NEJM199503093321001>.
8. Ravussin, Y., Leibel, R.L., and Ferrante, A.W. (2014). A Missing Link in Body Weight Homeostasis: The Catabolic Signal of the Overfed State. *Cell Metabol.* 20, 565–572. <https://doi.org/10.1016/j.cmet.2014.09.002>.
9. Lund, J., Lund, C., Morville, T., and Clemmensen, C. (2020). The unidentified hormonal defense against weight gain. *PLoS Biol.* 18, e3000629. <https://doi.org/10.1371/journal.pbio.3000629>.
10. Ahima, R.S., Prabakaran, D., Mantzoros, C., Qu, D., Lowell, B., Maratos-Flier, E., and Flier, J.S. (1996). Role of leptin in the neuroendocrine response to fasting. *Nature* 382, 250–252. <https://doi.org/10.1038/382250a0>.
11. Ravussin, Y., Edwin, E., Gallop, M., Xu, L., Bartolomé, A., Kraakman, M.J., LeDuc, C.A., and Ferrante, A.W. (2018). Evidence for a Non-leptin System that Defends against Weight Gain in Overfeeding. *Cell Metabol.* 28, 289–299.e5. <https://doi.org/10.1016/j.cmet.2018.05.029>.
12. Weisberg, S.P., Hunter, D., Huber, R., Lemieux, J., Slaymaker, S., Vaddi, K., Charo, I., Leibel, R.L., and Ferrante, A.W., Jr. (2006). CCR2 modulates inflammatory and metabolic effects of high-fat feeding. *J. Clin. Invest.* 116, 115–124. <https://doi.org/10.1172/JCI24335>.
13. Huang, Y., Hertzel, A.V., Fish, S.R., Halley, C.L., Bohm, E.K., Martinez, H.M., Durfee, C.C., Sanders, M.A., Harris, R.S., Niedernhofer, L.J., and Bernlohr, D.A. (2023). TP53/p53 Facilitates Stress-Induced Exosome and Protein Secretion by Adipocytes. *Diabetes* 72, 1560–1573. <https://doi.org/10.2337/db22-1027>.
14. Flaherty, S.E., Grjivalva, A., Xu, X., Ables, E., Nomanji, A., and Ferrante, A.W. (2019). A lipase-independent pathway of lipid release and immune modulation by adipocytes. *Science* 363, 989–993. <https://doi.org/10.1126/science.aaw2586>.
15. Ying, W., Riopel, M., Bandyopadhyay, G., Dong, Y., Birmingham, A., Seo, J.B., Ofrecio, J.M., Wollam, J., Hernandez-Carretero, A., Fu, W., et al. (2017). Adipose Tissue Macrophage-Derived Exosomal miRNAs Can Modulate In Vivo and In Vitro Insulin Sensitivity. *Cell* 171, 372–384.e12. <https://doi.org/10.1016/j.cell.2017.08.035>.
16. Brestoff, J.R., Wilen, C.B., Moley, J.R., Li, Y., Zou, W., Malvin, N.P., Rowen, M.N., Saunders, B.T., Ma, H., Mack, M.R., et al. (2021). Intercellular Mitochondria Transfer to Macrophages Regulates White Adipose Tissue Homeostasis and Is Impaired in Obesity. *Cell Metabol.* 33, 271–282. <https://doi.org/10.1016/j.cmet.2020.11.008>.
17. Borcherding, N., Jia, W., Giwa, R., Field, R.L., Moley, J.R., Kopecky, B.J., Chan, M.M., Yang, B.Q., Sabio, J.M., Walker, E.C., et al. (2022). Dietary lipids inhibit mitochondria transfer to macrophages to divert adipocyte-derived mitochondria into the blood. *Cell Metabol.* 34, 1499–1513.e8. <https://doi.org/10.1016/j.cmet.2022.08.010>.
18. Crewe, C., Funcke, J.-B., Li, S., Joffin, N., Gliniak, C.M., Ghaben, A.L., An, Y.A., Sadek, H.A., Gordillo, R., Akgul, Y., et al. (2021). Extracellular vesicle-based interorgan transport of mitochondria from energetically stressed adipocytes. *Cell Metabol.* 33, 1853–1868.e11. <https://doi.org/10.1016/j.cmet.2021.08.002>.

19. Chen, E.Y., Tan, C.M., Kou, Y., Duan, Q., Wang, Z., Meirelles, G.V., Clark, N.R., and Ma'ayan, A. (2013). Enrichr: interactive and collaborative HTML5 gene list enrichment analysis tool. *BMC Bioinf.* 14, 128. <https://doi.org/10.1186/1471-2105-14-128>.
20. Xie, Z., Bailey, A., Kuleshov, M.V., Clarke, D.J.B., Evangelista, J.E., Jenkins, S.L., Lachmann, A., Wojciechowicz, M.L., Kropiwnicki, E., Jagodnik, K.M., et al. (2021). Gene Set Knowledge Discovery with Enrichr. *Curr. Protoc.* 1, e90. <https://doi.org/10.1002/cpz1.90>.
21. Kuleshov, M.V., Jones, M.R., Rouillard, A.D., Fernandez, N.F., Duan, Q., Wang, Z., Koplev, S., Jenkins, S.L., Jagodnik, K.M., Lachmann, A., et al. (2016). Enrichr: a comprehensive gene set enrichment analysis web server 2016 update. *Nucleic Acids Res.* 44, W90–W97. <https://doi.org/10.1093/nar/gkw377>.
22. Rouault, C., Pellegrinelli, V., Schilch, R., Cotillard, A., Poitou, C., Tordjman, J., Sell, H., Clément, K., and Lacasa, D. (2013). Roles of Chemokine Ligand-2 (CXCL2) and Neutrophils in Influencing Endothelial Cell Function and Inflammation of Human Adipose Tissue. *Endocrinology* 154, 1069–1079. <https://doi.org/10.1210/en.2012-1415>.
23. Eguchi, A., Lazic, M., Armando, A.M., Phillips, S.A., Katebian, R., Maraka, S., Quehenberger, O., Sears, D.D., and Feldstein, A.E. (2016). Circulating adipocyte-derived extracellular vesicles are novel markers of metabolic stress. *J. Mol. Med.* 94, 1241–1253. <https://doi.org/10.1007/s00109-016-1446-8>.
24. Gene Ontology Consortium; Aleksander, S.A., Balhoff, J., Carbon, S., Cherry, J.M., Drabkin, H.J., Ebert, D., Feuermaier, M., Gaudet, P., Harris, N.L., and David, P.H. (2023). The Gene Ontology knowledgebase in 2023. *Genetics* 224, iyad031. <https://doi.org/10.1093/genetics/iyad031>.
25. Ashburner, M., Ball, C.A., Blake, J.A., Botstein, D., Butler, H., Cherry, J.M., Davis, A.P., Dolinski, K., Dwight, S.S., Eppig, J.T., et al. (2000). Gene Ontology: tool for the unification of biology. *Nat. Genet.* 25, 25–29. <https://doi.org/10.1038/75556>.
26. Binder, J.X., Pletscher-Frankild, S., Tsafou, K., Stolte, C., O'Donoghue, S.I., Schneider, R., and Jensen, L.J. (2014). COMPARTMENTS: unification and visualization of protein subcellular localization evidence. *Database* 2014, bau012. <https://doi.org/10.1093/database/bau012>.
27. Monzel, A.S., Enríquez, J.A., and Picard, M. (2023). Multifaceted mitochondria: moving mitochondrial science beyond function and dysfunction. *Nat. Metab.* 5, 546–562. <https://doi.org/10.1038/s42255-023-00783-1>.
28. Subramanian, A., Tamayo, P., Mootha, V.K., Mukherjee, S., Ebert, B.L., Gillette, M.A., Paulovich, A., Pomeroy, S.L., Golub, T.R., Lander, E.S., and Mesirov, J.P. (2005). Gene set enrichment analysis: A knowledge-based approach for interpreting genome-wide expression profiles. *Proc. Natl. Acad. Sci. USA* 102, 15545–15550. <https://doi.org/10.1073/pnas.0506580102>.
29. Rath, S., Sharma, R., Gupta, R., Ast, T., Chan, C., Durham, T.J., Goodman, R.P., Grabarek, Z., Haas, M.E., Hung, W.H.W., et al. (2021). MitoCarta3.0: an updated mitochondrial proteome now with sub-organelle localization and pathway annotations. *Nucleic Acids Res.* 49, D1541–D1547. <https://doi.org/10.1093/nar/gkaa1011>.
30. Liu, L., Shah, S., Fan, J., Park, J.O., Wellen, K.E., and Rabinowitz, J.D. (2016). Malic enzyme tracers reveal hypoxia-induced switch in adipocyte NADPH pathway usage. *Nat. Chem. Biol.* 12, 345–352. <https://doi.org/10.1038/nchembio.2047>.
31. Song, Z., Xiaoli, A.M., and Yang, F. (2018). Regulation and Metabolic Significance of De Novo Lipogenesis in Adipose Tissues. *Nutrients* 10, 1383. <https://doi.org/10.3390/nu10101383>.
32. Martínez-Reyes, I., and Chandel, N.S. (2020). Mitochondrial TCA cycle metabolites control physiology and disease. *Nat. Commun.* 11, 102. <https://doi.org/10.1038/s41467-019-13668-3>.
33. Spees, J.L., Olson, S.D., Whitney, M.J., and Prockop, D.J. (2006). Mitochondrial transfer between cells can rescue aerobic respiration. *Proc. Natl. Acad. Sci. USA* 103, 1283–1288. <https://doi.org/10.1073/pnas.0510511103>.
34. Tiash, S., Brestoff, J.R., and Crewe, C. (2023). A guide to studying mitochondria transfer. *Nat. Cell Biol.* 25, 1551–1553. <https://doi.org/10.1038/s41556-023-01246-1>.
35. Rosina, M., Ceci, V., Turchi, R., Chuan, L., Borcherding, N., Sciarretta, F., Sánchez-Díaz, M., Tortolici, F., Karlinsey, K., Chiurchiù, V., et al. (2022). Ejection of damaged mitochondria and their removal by macrophages ensure efficient thermogenesis in brown adipose tissue. *Cell Metabol.* 34, 533–548.e12. <https://doi.org/10.1016/j.cmet.2022.02.016>.
36. Xu, X., Grijalva, A., Skowronski, A., van Eijk, M., Serlie, M.J., and Ferrante, A.W. (2013). Obesity activates a program of lysosomal-dependent lipid metabolism in adipose tissue macrophages independently of classic activation. *Cell Metabol.* 18, 816–830. <https://doi.org/10.1016/j.cmet.2013.11.001>.
37. Grijalva, A., Xu, X., and Ferrante, A.W. (2016). Autophagy Is Dispensable for Macrophage-Mediated Lipid Homeostasis in Adipose Tissue. *Diabetes* 65, 967–980. <https://doi.org/10.2337/db15-1219>.
38. Gabriely, I., Ma, X.H., Yang, X.M., Atzmon, G., Rajala, M.W., Berg, A.H., Scherer, P., Rossetti, L., and Barzilai, N. (2002). Removal of Visceral Fat Prevents Insulin Resistance and Glucose Intolerance of Aging: An Adipokine-Mediated Process? *Diabetes* 51, 2951–2958. <https://doi.org/10.2337/diabetes.51.10.2951>.
39. Börgeson, E., Boucher, J., and Hagberg, C.E. (2022). Of mice and men: Pinpointing species differences in adipose tissue biology. *Front. Cell Dev. Biol.* 10, 1003118.
40. Guo, D.-H., Yamamoto, M., Hernandez, C.M., Khodadadi, H., Baban, B., and Stranahan, A.M. (2021). Beige adipocytes mediate the neuroprotective and anti-inflammatory effects of subcutaneous fat in obese mice. *Nat. Commun.* 12, 4623. <https://doi.org/10.1038/s41467-021-24540-8>.
41. Kamogawa, K., Kohara, K., Tabara, Y., Uetani, E., Nagai, T., Yamamoto, M., Igase, M., and Miki, T. (2010). Abdominal Fat, Adipose-Derived Hormones and Mild Cognitive Impairment: The J-SHIPP Study. *Dement. Geriatr. Cogn. Disord.* 30, 432–439. <https://doi.org/10.1159/000321985>.
42. Chusyd, D.E., Wang, D., Huffman, D.M., and Nagy, T.R. (2016). Relationships between Rodent White Adipose Fat Pads and Human White Adipose Fat Deposits. *Front. Nutr.* 3, 10. <https://doi.org/10.3389/fnut.2016.00010>.
43. Meier, F., Brunner, A.-D., Frank, M., Ha, A., Bludau, I., Voytik, E., Kaspar-Schoenefeld, S., Lubeck, M., Raether, O., Bache, N., et al. (2020). diaPA-SEF: parallel accumulation–serial fragmentation combined with data-independent acquisition. *Nat. Methods* 17, 1229–1236. <https://doi.org/10.1038/s41592-020-00998-0>.
44. Kulak, N.A., Pichler, G., Paron, I., Nagaraj, N., and Mann, M. (2014). Minimal, encapsulated proteomic-sample processing applied to copy-number estimation in eukaryotic cells. *Nat. Methods* 11, 319–324. <https://doi.org/10.1038/nmeth.2834>.
45. Bruderer, R., Bernhardt, O.M., Gandhi, T., Miladinović, S.M., Cheng, L.-Y., Messner, S., Ehrenberger, T., Zanotelli, V., Butscheid, Y., Escher, C., et al. (2015). Extending the Limits of Quantitative Proteome Profiling with Data-Independent Acquisition and Application to Acetaminophen-Treated Three-Dimensional Liver Microtissues. *Mol. Cell. Proteomics* 14, 1400–1410. <https://doi.org/10.1074/mcp.M114.044305>.
46. Bonnot, T., Gillard, M., and Nagel, D. (2019). A Simple Protocol for Informative Visualization of Enriched Gene Ontology Terms. *Bio-Protoc. Bio. Protoc.* 9, e3429. <https://doi.org/10.21769/BioProtoc.3429>.
47. Marini, F., and Binder, H. (2019). pcaExplorer: an R/Bioconductor package for interacting with RNA-seq principal components. *BMC Bioinf.* 20, 331. <https://doi.org/10.1186/s12859-019-2879-1>.

STAR★METHODS

KEY RESOURCES TABLE

REAGENT or RESOURCE	SOURCE	IDENTIFIER
Antibodies		
Rabbit monoclonal anti-adiponectin	Invitrogen	Cat# 11H4L4; RRID: AB_2532410
Mouse monoclonal anti-beta-actin	Sigma-Aldrich	Cat# A5441; RRID: AB_476744
Rabbit polyclonal anti-COXIV	Abcam	Cat# ab16056; RRID: AB_443304
Rabbit monoclonal anti-HSP60	Abcam	Cat# ab190828; RRID: AB_2814692
Rabbit polyclonal anti-ME1	Abcam	Cat# ab97445; RRID: AB_10679994
Rabbit monoclonal anti-ME2	Abcam	Cat# ab139686
Rabbit monoclonal anti-TOM20	Abcam	Cat# ab186735; RRID: AB_2889972
Horse anti-mouse IgG HRP	Vector Labs	Cat# PI-2000-1; RRID: AB_2336177
Donkey anti-rabbit IgG HRP	Invitrogen	Cat# A16023; RRID: AB_2534697
Chemicals, peptides, and recombinant proteins		
Recombinant human M-CSF	R&D Systems	Cat# 216-MC
Critical commercial assays		
iQ SYBR Green Supermix	Bio-Rad	Cat# 1708882
Deposited data		
Proteomics data	ProteomeXchange, PRIDE	PXD051294, PXD051296
Experimental models: Organisms/strains		
B6.BKS(D)-Lepr ^{db} /J mice	The Jackson Laboratory	Cat# 000697
C57BL/6J mice	The Jackson Laboratory	Cat# 000664
Oligonucleotides		
mMito1 F: CTAGAAACCCCGAAACCAAA	Life Technologies	N/A
mMito1 R: CCAGCTATCACCAAGCTCGT	Life Technologies	N/A
B2m F: ATGGGAAGCCGAACATACTG	Life Technologies	N/A
B2m R: CAGTCTCAGTGGGGGTGAAT	Life Technologies	N/A
Software and algorithms		
BioRender	BioRender	N/A
FlowJo (v10.10)	BD	N/A
Prism (v10.4)	GraphPad	N/A
Enrichr	Ma'ayan Lab	N/A
R (v3.6.2)	R Core Team	N/A
RStudio (v2023.06.0)	Posit PBC	N/A
pcaExplorer (v2.12.0)	Federico Marini	N/A
ggplot2 (v3.5.1)	Hadley Wickham	N/A
Other		
Low-fat diet (PicoLab Rodent Diet 20)	LabDiet	Cat# 5053
High-fat diet	Research Diets	Cat# D12492i
Sephacryl® S-500 HR	Cytiva	Cat# 17-0613-10
ViewSizer 3000	MANTA Instruments, Horiba Scientific	N/A
JEM 1400 electron microscope	JEOL	N/A
LSRFortessa	BD	N/A

EXPERIMENTAL MODEL AND STUDY PARTICIPANT DETAILS

Animals and animal care

C57BL/6J and B6.BKS(D)-*Lepr*^{db}/J mice were obtained from The Jackson Laboratory (Bar Harbor, ME). Mice were singly housed in a non-barrier facility. Low-fat pellet diet contained 5% calories from fat (PicoLab Rodent Diet 20; Purina Mills Inc) while high-fat pellet diet contained 60% calories from fat (D12492i; Research Diets Inc). Mice were between 12 and 16 weeks of age at time of sacrifice and analysis. Mice were randomly assigned to experimental groups when comparing animals of the same genetic background. Animal procedures were approved by Columbia University Institutional Animal Care and Use Committee. All mice are male unless otherwise noted. All mice were age-matched within comparisons with the exception of *db/db* mice owing to the differential rates of weight gain between *db/db* and B6 mice (including B6 mice fed a high-fat diet), in which case mice were weight-matched rather than age-matched, as described in the text.

Adipose tissue culture

Murine perigonadal adipose tissue depots were cultured in Minimum Essential Medium Alpha (MEM-a, Gibco, 41061029) with 1% penicillin/streptomycin at 37°C and 5% CO₂.

Macrophage culture

Bone marrow cells were collected from the femurs and tibias of 12-week-old male C57BL/6J mice. Cells were washed, counted, and plated at 50 million cells per 175 mL tissue culture flask in bone marrow culture medium (MEM- α with 10% FBS, 1% non-essential amino acids (Invitrogen) and 1% penicillin) at 37°C, 5% CO₂. After two days in culture, viable non-adherent cells were collected, counted, and plated in 23mm (12-well) tissue culture dishes in 2 mL of culture medium supplemented with 30 ng/mL human M-CSF (R&D Systems). After two days of differentiation in the presence of M-CSF, media was removed, cells were washed 3x with PBS, and fresh culture medium supplemented with M-CSF was added. After an additional two days in culture, cells were washed and supplemented with PKH26-labeled adipose tissue-derived EVs or PKH26-labeled adipose tissue-derived mitochondria for an hour, after which they were washed again, collected, stained with DAPI, and taken for FACS analysis. Testing of our primary cell cultures for mycoplasma contamination was not completed.

METHOD DETAILS

Surgery

Animals were fasted overnight and then refed early in the morning so as to have a fuller stomach at the time of surgery (mice were given at least 2 h to feed before undergoing surgery). The animals were anesthetized using inhaled isoflurane (using a SomnoSuite, Kent Scientific, Torrington, CT) and surgical sites (interscapular and ventral regions) shaved and prepped in a sterile manner. For pre-surgical pain control, buprenorphine (0.05 mg/kg), carprofen (5 mg/kg) and bupivacaine (2 mg/kg) were administered subcutaneously after induction of anesthesia. Carprofen injections were repeated every 24 h for 3 days during the recovery period. A small (8–12 mm) incision was made along the midline from the base of the skull down to interscapular region. Surgical scissors and a curved hemostat were used to separate the skin from the underlying muscle tissue around the incision site and extending toward the left flank to create a subcutaneous tunnel. A ventral incision below the xiphoid was made down through the mid-abdomen so that the stomach could be accessed. The stomach was then gently withdrawn from the abdomen, externally stabilized with sterile gauze and positioned so that the fundus was along the superior midline. After centrally aligning the intragastric tube and mesh atop the fundus, a polypropylene suture (Covidien Medtronic, cat. No. VP-556-X) was threaded through both the stomach and the mesh and tied into a loose knot. A small puncture was made into the ventral forestomach using a sterile 18G needle in order to facilitate the insertion of the angled end of the Micro-Renathane tube. Once confirmed to be properly inset into the fundus the first suture was tightened and 3 more equidistant sutures were added to firmly affix the mesh to the stomach. To ensure there were no leaks, 200 mL of sterile saline was infused through the tube using a 22G needle and syringe. The longer end of the tube was then passed through an incision in the peritoneal wall on the left side of the animal. The incision was made using jewelry tweezers passed through the previously established subcutaneous tunnel. The peritoneal and abdominal incisions were then closed using 5-0 Monofilament Nylon (Covidien Medtronic, cat. No. SN-871) sutures and skin clips respectively. After flipping the animal so that the posterior interscapular region was accessible, the tube was attached to the vascular button (Instech, cat. No. VAB62BS/22) which was sutured to the interscapular muscles under the skin. The interscapular incision was then sutured closed using 5-0 Monofilament Nylon sutures. Triple antibiotic ointment (bacitracin, neomycin, and polymyxin B) was applied to the catheter exit wounds daily for 3 days to prevent infection. Mice infusions started 1–3 weeks post-surgery depending on experiment.

Intragastric tube preparation

Micro-Renathane tubes (Braintree Scientific, cat. No. MRE 037) approx. 12 cm long were threaded through approx. 1 cm² square pieces of mesh (Bard Mesh Monofilament Polypropylene Davol, cat. No. 0112660) using a jewelry tweezer leaving one side with approx. 1.5 cm of tubing and affixed together with Krazy glue. Prior to surgery, the mesh was cut into small circles while simultaneously

ensuring there were at least four needle-sized holes for sutures. The smaller side of the tube was cut on an angle yielding 0.5–0.75 cm length of tube that could be placed into the fundus of the stomach.

Overfeeding protocol

After acclimatization to the Columbia mouse facilities (exact duration dependent on the specific experiment but between 1 and 4 weeks), wild-type mice underwent gastric tube implantation surgery (see above) and were allowed to recover for at least 1 week before initiation of overfeeding. Ensure or saline infusion was performed for 12 days. Mice were excluded and euthanized if surgery was unsuccessful or the feeding system clogged and could not be used. During the feeding protocol the Vanilla Ensure original powder (Abbott Laboratories Chicago, IL) was reconstituted in deionized water to obtain a 0.92 kcal/mL liquid for use in intra-gastric feeding experiments (24 g of powder was mixed with 100 mL of water). To prevent congealing of the liquid diet and clogging of the feeding tubes, the diet was prepared fresh daily and kept at 4°C until infusions were begun. Infusions were conducted for 14 h coinciding with the dark cycle, beginning at 20 h and finishing at 10 h the next morning. At 10 h in the morning, following overnight infusion, 1 mL of water was flushed through the diet delivery tubes (to prevent diet buildup and subsequent clogging) and mice were weighed immediately thereafter. During overfeeding experiments, infusion of calories began as low as 11 kcal/day and was slowly increased to a maximum of 24 kcal/day. After 11 days of infusions, at which point body weights of the overfed and control populations were equal, mice were fasted overnight and then sacrificed. All studies were approved by the Columbia University Institutional Animal Care and Use Committee.

Processing of conditioned media

Perigonadal adipose tissue depots were taken from mice, minced in warm phosphate-buffered saline (PBS), centrifuged at 500g for 5 min to pellet vasculature or other non-adipose contaminants, and cultured in Minimum Essential Medium Alpha (MEM-a, Gibco, 41061029) with 1% penicillin/streptomycin at 37°C and 5% CO₂. After 6 h, conditioned media were collected, passed through a 70µm filter (Greiner Bio-One, 542070) to exclude large tissue chunks, and passed through a 0.8µm syringe filter (Sartorius, 16592) to exclude cells. Protease inhibitor (Sigma-Aldrich, P8340) was added 1:100 and the media were frozen at -80°C. 100% trichloroacetic acid (TCA) solution was generated by dissolving 100g of TCA (Sigma-Aldrich, T6399) in 45.4 mL ultra-pure distilled water. After thawing conditioned media samples, 176 µL of 100% TCA was mixed with 1 mL conditioned media to achieve a final concentration of 15% TCA (v/v), and samples were incubated on ice. After 3 h of incubation, samples were centrifuged for 15 min at 20,000 g at 4°C, after which TCA was aspirated off. Protein pellets were then washed with 1 mL cold acetone (Sigma-Aldrich, 179124) and again centrifuged; this was repeated four times, after which acetone was aspirated off and pellets were allowed to briefly air dry.

Global quantitative proteomics analysis

For the global quantitative proteomic analysis of secretomes from mouse perigonadal adipose tissue (PGAT) under different metabolic conditions (*ad libitum* obesity (ALO) and overfeeding-induced obesity (OIO)), diaPASEF⁴³ based proteomics was employed. In brief, TCA precipitated samples were denatured in SDC buffer⁴⁴ (1% SDC, and 100 mM TrisHCl pH 8.5) and boiled for 15 min at 60°C, 1000 rpm. Protein reduction and alkylation of cysteins, was performed with 10 mM TCEP and 40 mM CAA at 45°C for 10 min followed by sonication in a water bath, cooled down to room temperature. Protein digestion was processed for overnight by adding LysC/ trypsin mix in a 1:50 ratio (µg of enzyme to µg of protein) at 37°C and 1400 rpm. Peptides were acidified by adding 1% TFA, vortexed, and subjected to StageTip clean-up via SDB-RPS² and dried in a speed-vac. Peptides were resuspended in 10 µL of LC buffer (3% ACN/0.1% FA). Peptide concentrations were determined using NanoDrop and 200 ng of each sample were used for diaPASEF analysis on timsTOFPro.

The default settings were used for targeted analysis of DIA data in Spectronaut except the decoy generation was set to mutate. The false discovery rate (FDR) was estimated with the mProphet approach and set to 1% at the peptide precursor level and 1% at the protein level. The label-free quantitation (LFQ) intensities were further analyzed using the Spectronaut statistical package. Significantly changed protein abundance was determined by unpaired t test with a threshold for significance of $p < 0.05$ (permutation-based FDR correction) and 0.58 log2FC.

LC-MS/MS

Peptides were separated within 87 min at a flow rate of 400 nL/min on a reversed-phase C18 column with an integrated CaptiveSpray Emitter (25 cm × 75µm, 1.6 µm, IonOpticks). Mobile phases A and B were with 0.1% formic acid in water and 0.1% formic acid in ACN. The fraction of B was linearly increased from 2 to 23% within 70 min, followed by an increase to 35% within 10 min and a further increase to 80% before re-equilibration. The timsTOF Pro was operated in diaPASEF mode and data was acquired at defined 32 × 50 Th isolation windows from m/z 400 to 1,200. To adapt the MS1 cycle time in diaPASEF, set the repetitions to 2 in the 16-scan diaPASEF scheme. The collision energy was ramped linearly as a function of the mobility from 59 eV at 1/K₀ = 1.6 Vs. cm⁻² to 20 eV at 1/K₀ = 0.6 Vs. cm⁻². The acquired diaPASEF raw files were searched with the UniProt Mouse proteome database in the Spectronaut Pulsar X,⁴⁵ a mass spectrometer vendor-independent software from Biognosys. The default settings were used for targeted analysis of DIA data in Spectronaut except the decoy generation was set to mutate. The false discovery rate (FDR) was estimated with the mProphet approach and set to 1% at the peptide precursor level and 1% at the protein level. The label-free quantitation (LFQ)

intensities were further analyzed using the Spectronaut statistical package. Significantly changed protein abundance was determined by unpaired t test with a threshold for significance of $p < 0.05$ (permutation-based FDR correction) and 0.58 log2FC.

Exosome enrichment

Perigonadal adipose tissue was taken from mice, minced to ~2mm chunks, and cultured in Minimum Essential Medium Alpha (MEM-a, Gibco, 41061029) with 1% penicillin/streptomycin for 16–20 h. Conditioned media were passed through a 70 μ m filter (Greiner Bio-One, 542070) and collected. The medium was then passed through a 0.8 μ m syringe filter (Sartorius, 16592) and concentrated via 100kDa centrifuge filters (Millipore, UFC210024) via centrifugation at 3000 g at 4°C. For column testing and validation, the concentrated conditioned medium was then labeled with PKH26 (Sigma-Aldrich, PKH26GL) according to manufacturer's instructions; for collection of fractions from already-validated columns, concentrated conditioned medium was left unlabeled. The medium was added to a gel filtration column (Thermo Scientific, 29922) packed with Sepharose beads (Cytiva, 17061310), using PBS as the mobile phase. 500 μ L fractions of eluate from the column were collected. For column validation, the fluorescent emission of labeled exosomes was measured using a Varioskan LUX fluorescence spectrophotometer plate reader (Thermo Fisher). The fractions corresponding with the peak in PKH26 fluorescence were subsequently used when collecting exosomes from unlabeled samples.

For isolation of the crude intact mitochondrial fraction, adipose tissue was placed in PBS with protease inhibitor (Sigma-Aldrich, P8340, 1:100 dilution) and gently dissociated using a pellet mixer (VWR, 47747-370). Homogenate was centrifuged at 1500g for 5 min at 4° and the aqueous fraction was taken and spun at 15,000g for 5 min at 4°. The supernatant was then aspirated off and the pellet gently resuspended in PBS with protease inhibitor for further analysis.

Nanoparticle tracking analysis

Purified exosome samples were analyzed for particle concentration and size distribution using nanoparticle tracking analysis with the ViewSizer 3000 (MANTA Instruments, Horiba Scientific). The assays were performed according to the recommended protocols of the manufacturer. Concentrated exosome preparations were diluted in PBS and 50 15s tracking measurements were captured at room temperature for each sample. The measurements were then analyzed using in-built Viewsizer software using PBS as a control.

Western blot

For analysis of whole-tissue protein, tissue was placed in RIPA buffer containing protease inhibitor (Sigma-Aldrich, P8340) in tubes containing zirconium beads (Sigma-Aldrich, Z763802) and homogenized (Fisher Scientific, Bead Mill 24). Samples were subsequently centrifuged at 1500g for 5 min at 4° to pellet debris, and the aqueous fraction was taken for further analysis.

For Western blots comparing SEC fractions, equal volumes of each sample were loaded. For all other Western blots, equal weights of protein were loaded in each lane as assessed via BCA assay (Thermo Fisher, 23227).

Samples were denatured in Laemmli SDS sample buffer (Thermo Scientific, J61337AC) at 100°C for 15 min and run on a 4–20% gradient polyacrylamide gel (Bio-Rad, 4561094 and 4561096) at 110V for 70–100 min. Proteins were transferred to PVDF (Millipore, IPVH00010) at 65V for 50 min using a wet transfer system containing methanol-free transfer buffer (Thermo Fisher, 35045). Membranes were blocked with 5% non-fat milk in tris-buffered saline with Tween (TBST, Thermo Fisher, 28360) or with SuperBlock (Thermo Fisher, 37536) and then incubated with primary antibodies overnight. Membranes were washed with TBST, incubated with horseradish peroxidase-conjugated secondary antibodies for an hour, and washed. Visualization was completed using an enhanced chemiluminescent substrate (Thermo Fisher, 34577).

Primary antibody against TOM20 (Abcam, ab186735) was used at 1:100 dilution. Primary antibodies against adiponectin (Invitrogen, 11H4L4) and ME2 (Abcam, ab139686) were used at 1:500 dilution. Primary antibodies against COXIV (Abcam, ab16056), HSP60 (Abcam, ab190828), and ME1 (Abcam, ab97445), as well as secondary antibodies against mouse IgG (Vector Labs, PI-2000-1) and rabbit IgG (Invitrogen, A16023), were used at 1:1000 dilution. Primary antibody against beta-actin (Sigma-Aldrich, A5441) was used at 1:5000 dilution.

qPCR

Quantitative polymerase chain reaction of DNA from conditioned media was performed using iQ SYBR Green Supermix (Bio-Rad, 1708882). 2 μ L of conditioned media collected as described above was used as a template for each reaction, with 10 μ L of the Supermix used in addition to 7 μ L of water and 1 μ L of 10 mM primer mix. Reactions were run using a CFX Connect Real-Time Detection System (Bio-Rad) using a total volume of 20 μ L per well on a white 96-well plate (Bio-Rad, MLL-9651) following kit instructions.

Electron microscopy

Adipose tissue was cultured as described overnight as described above. Conditioned media was taken and passed through a 70 μ m filter, after which it was centrifuged at 1500 g at 4°C for 5 min to pellet debris. Supernatant was collected and centrifuged for an additional 5 min at 15,000 g at 4°C to pellet mitochondrial material. Supernatant was gently removed so as not to disturb the pellet, and a fixative solution (2.5% glutaraldehyde, 4% paraformaldehyde, 0.02% picric acid in 0.1M sodium cacodylate buffer, pH 7.3) was added and the samples were fixed for between 24 h and 10 days at 4°C. Following fixation, pellets were washed in 0.1M sodium cacodylate buffer and post-fixed in aqueous 1% OsO₄, 1.5%K-ferricyanide for 1 h. Following post-fixation, pellets were again washed in 0.1M sodium cacodylate buffer and dehydrated through a graded ethanol series followed by acetonitrile for 15 min per

step. Pellets were then infiltrated and embedded in Embed 812 resin (Electron Microscopy Sciences, #14900). Resin was polymerized at 50°C for 24 h. Sample blocks were trimmed and sections cut at 65–70 nm (silver-gold) using a Diatome diamond knife on a Leica Ultracut S ultramicrotome. Sections were contrasted with lead citrate and viewed on a JEM 1400 electron microscope (JEOL) operated at 100 kV. Digital images were recorded using a Veleta 2 K × 2 K camera (EMSIS).

Flow cytometry

FACS was performed using an LSRII Fortessa (BD). All samples were gated on size and to exclude doublets and DAPI+ cells prior to analysis. Data analysis was performed using FlowJo (BD).

Figures

Figures were constructed using BioRender, FlowJo (BD), and Prism 10 (GraphPad). Gene set enrichment diagrams were made in R using a published protocol.⁴⁶ Principal component analysis and associated diagrams were completed using pcaExplorer.⁴⁷ Ovals around groups represent 95% confidence intervals.

QUANTIFICATION AND STATISTICAL ANALYSIS

Data are expressed as means ± SEM and exact statistical parameters can be found for each experiment in the figure legends. ImageJ (NIH) was used for quantification of Western blot intensity. Statistical significance was determined utilizing Student's t-test and ANOVA using Prism 10 and Microsoft Excel. Benjamini-Hochberg was used for multiple-comparison correction. Significance was considered $p < .05$.